ORNL/NUREG/TM-100

Inference of Core Barrel Motion from Neutron Noise Spectral Density

J. C. Robinson
F. Shahrokhi
R. C. Kryter

Prepared for the U.S. Nuclear Regulatory Commission
Office of Nuclear Reactor Regulation
Under Interagency Agreement ERDA (40-544-75)

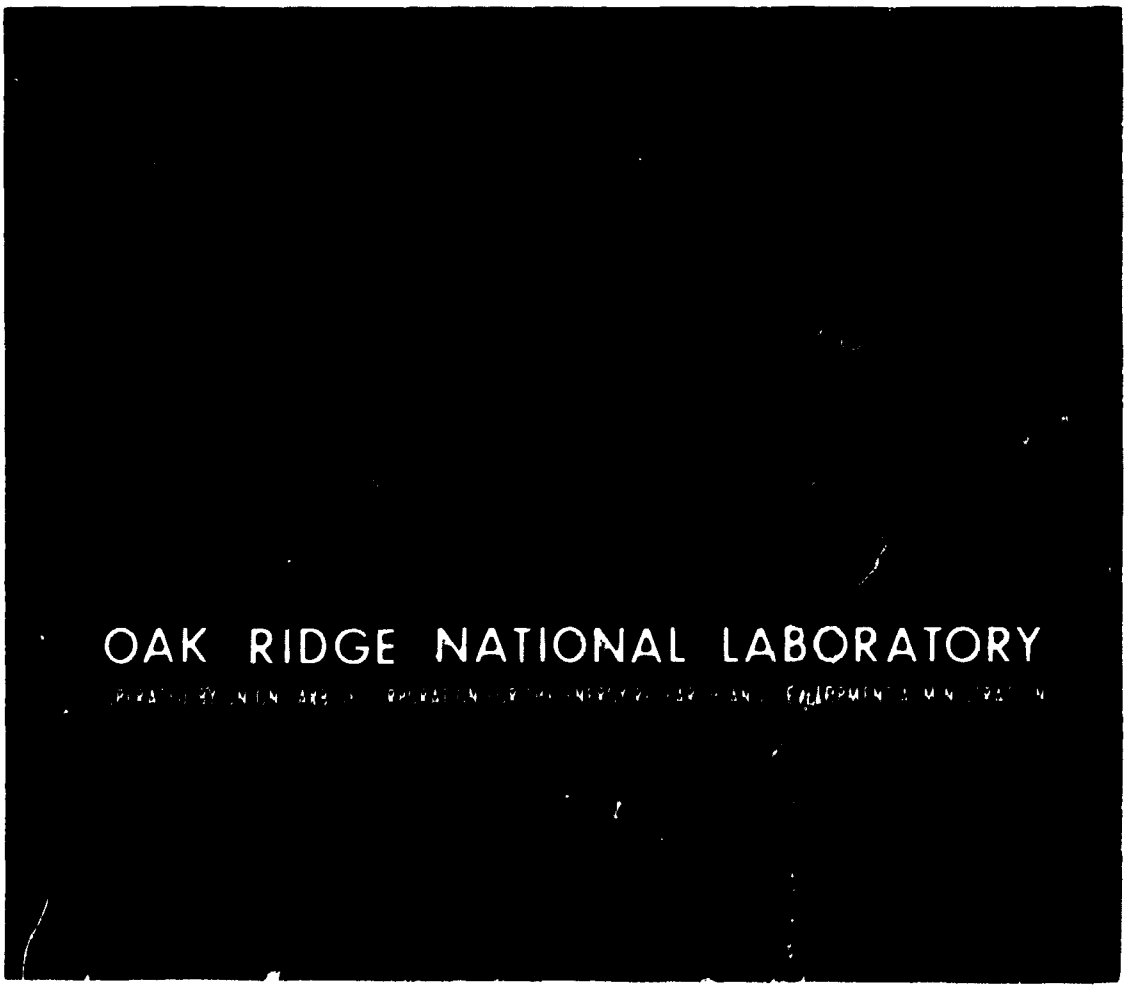

BLANK PAGE

Printed in the United States of America Available from
National Technical Information Service
U.S. Department of Commerce
5285 Port Royal Road, Springfield, Virginia 22161
Price: Printed Copy $4.50; Microfiche $3.00

ORNL/NUREG/TM-100
Dist. Category NRC-1

Contract No. W-7405-eng-26

INSTRUMENTATION AND CONTROLS DIVISION

INFERENCE OF CORE BARREL MOTION FROM NEUTRON NOISE SPECTRAL DENSITY

J. C. Robinson* F. Shahrokhi** R. C. Kryter

*Consultant, Nuclear Engineering Department, the University of Tennessee, Knoxville 37916.

**Graduate student, Nuclear Engineering Department, the University of Tennessee, Knoxville 37916.

Manuscript Completed - March 15, 1977

Date Published - April 1977

Prepared for the
U.S. Nuclear Regulatory Commission
Office of Nuclear Reactor Regulation
Under Interagency Agreement ERDA (40-544-75)

Prepared by the
OAK RIDGE NATIONAL LABORATORY
Oak Ridge, Tennessee 37830
operated by
UNION CARBIDE CORPORATION
for the
ENERGY RESEARCH AND DEVELOPMENT ADMINISTRATION

ABSTRACT

A method was developed for inference of core barrel motion from the following statistical descriptors: cross-power spectral density, auto-power spectral density, and amplitude probability density. To quantify the core barrel motion in a typical pressurized water reactor (PWR), a scale factor was calculated in both one- and two-dimensional geometries using forward, variational, and perturbation methods of discrete ordinates neutron transport. A procedure for selection of the proper frequency band limits for the statistical descriptors was developed.

We found that although perturbation theory is adequate for the calculation of the scale factor, two-dimensional geometric effects are important enough to rule out the use of a one-dimensional approximation for all but the crudest calculations. We also found that contributions of gamma rays can be ignored and that the results are relatively insensitive to the cross-section set employed.

The proper frequency band for the statistical descriptors is conveniently determined from the coherence and phase information from two ex-core power range neutron monitors positioned diametrically across the reactor vessel. Core barrel motion can then be quantified from the integral of the band-limited cross-power spectral density of two diametrically opposed ex-core monitors or, if the coherence between the pair is $\gtrsim 0.7$, from a properly band-limited amplitude probability density function. Wide-band amplitude probability density functions were demonstrated to yield erroneous estimates for the magnitude of core barrel motion.

CONTENTS

1. INTRODUCTION

The methodology of inferring the magnitude of core support barrel movement in a pressurized water reactor (PWR) from statistical descriptors was developed and systematically analyzed. Such techniques and numerical values based on noise analysis of ex-core power range channel signals are of great interest to PWR manufacturers[1] and to the Nuclear Regulatory Commission (NRC)[2] because this methodology enables nonperturbative in-service monitoring for excessive mechanical motion of the reactor core support barrel, which might be indicative of degraded structural integrity. Nominally, using statistical analysis techniques, one obtains either amplitude probability density (APD) functions or normalized power spectral density (NPSD) functions from the fluctuating component of the signal from ex-core power range channels. A scale factor is calculated to convert these statistical descriptors into core barrel motion. However, there are potential pitfalls that can lead to serious error, especially underestimation of the core barrel motion, that is, pitfalls due to one-dimensional calculations and insufficient bandlimiting in the manner in which the APDs or NPSDs are constructed and the manner in which the scale factor is obtained. For this reason, the authors critically analyzed both the procedures used in calculating the scale factor and the selection of the proper band limits of the spectral density data.

2. BACKGROUND OF PROBLEM

This work was done at the specific request of the Division of Operating Reactors of the U.S. Nuclear Regulatory Commission. Among other things, this Division (1) establishes "branch positions" regarding

BLANK PAGE

the manner in which certain safety-related operational problems will be handled, and (2) reviews requests from licensees (utilities) who seek to change the manner in which they acquire and report certain safety-related plant data and to modify established operating practices. The work described in this report relates to both functions.

Excessive core barrel motion is judged a potential safety problem for PWRs. Monitoring the signals from existing ex-core neutron detectors is a simple and nonperturbative means of ensuring continued mechanical integrity of the pressure vessel internals. However, if monitoring is to be effective, the PWR plant operator must not only monitor the signals for changes in character over the plant's operating life, but the operator must also be able to infer the magnitude of the structural movement implied by the signal received so that mechanical engineers can decide whether the movement is acceptable from a structural fatigue point of view. The scale factor (SF) is the value that relates structural movement to the signals produced by ex-core detectors; hence, it is important to be able to place confidence in this number, which is not readily obtained experimentally (hence by calculation). This paper describes how to perform such calculation, including the many pitfalls.

Most attempts to date by reactor vendors to calculate SF values have neglected important effects, and, as a result, these values have been in error in the nonconservative direction, i.e., they underpredicted the amount of core barrel motion. For this reason, this methodology was developed and this document was prepared for the NRC to use in reviewing licensee proposals and to establish their branch position on this matter.

These issues are very important to the reactor industry and to the NRC, because the economics are large: to shut down one plant for one day as a result of suspected abnormal core barrel motion would cost a utility $300-500 thousand for replacement power.

3. CORE SUPPORT BARREL MOTION IN A PWR

The core in a PWR is supported by a core support barrel which is, in turn, supported by the reactor pressure vessel (hereafter referred to as core barrel and pressure vessel, respectively) at the vessel head (Fig. 1). The pressure vessel is supported by pads on the building foundation. Coolant flow enters the pressure vessel horizontally through four inlet nozzles (90° separation) at an elevation above the reactor core. The core barrel turns the coolant flow downward to the inlet plenum below the core. The coolant flows upward through the core and exits through two nozzles that penetrate the core barrel at nominally the same elevation as the inlet nozzles. (Figure 2 is a cross-sectional view of the pressure vessel at the flow entrance-exit elevation.)

From consideration of the way the core barrel is supported and the hydraulic forces on the pressure vessel at the inlet nozzles (Figs. 1 and 2), it is plausible that the core barrel will tend to move as a pendulum. If the core barrel does execute such a motion, then the force will be transmitted (as pointed out by Oesterle et al.[3]) to the pressure vessel which rests on building foundation pads (Fig. 1). Thus, the pressure vessel could also move as a pendulum. The net effect would be a double pendulum motion, as indicated in Fig. 1.

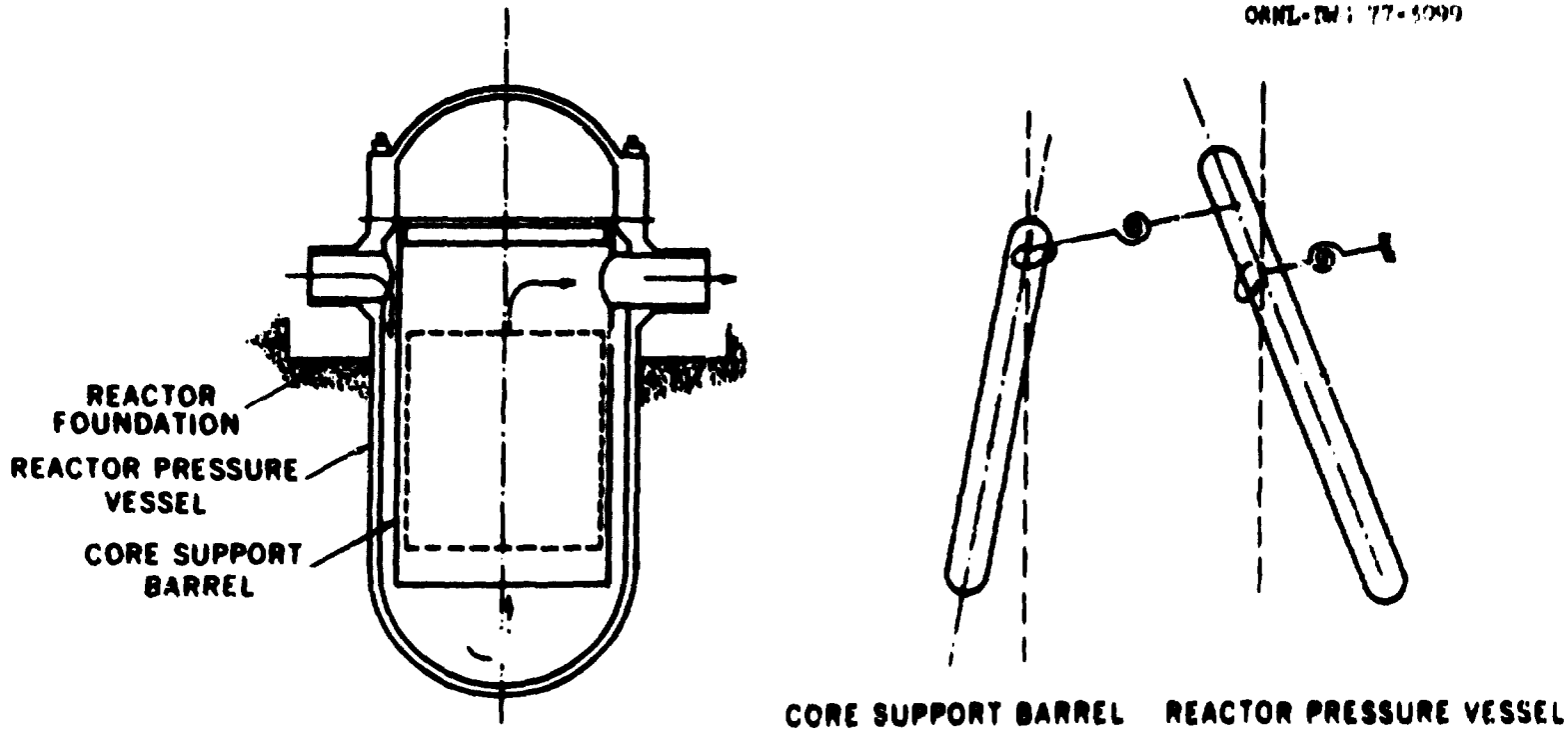

Fig. 1. A typical PWR reactor core structure and the double pendulum motion.

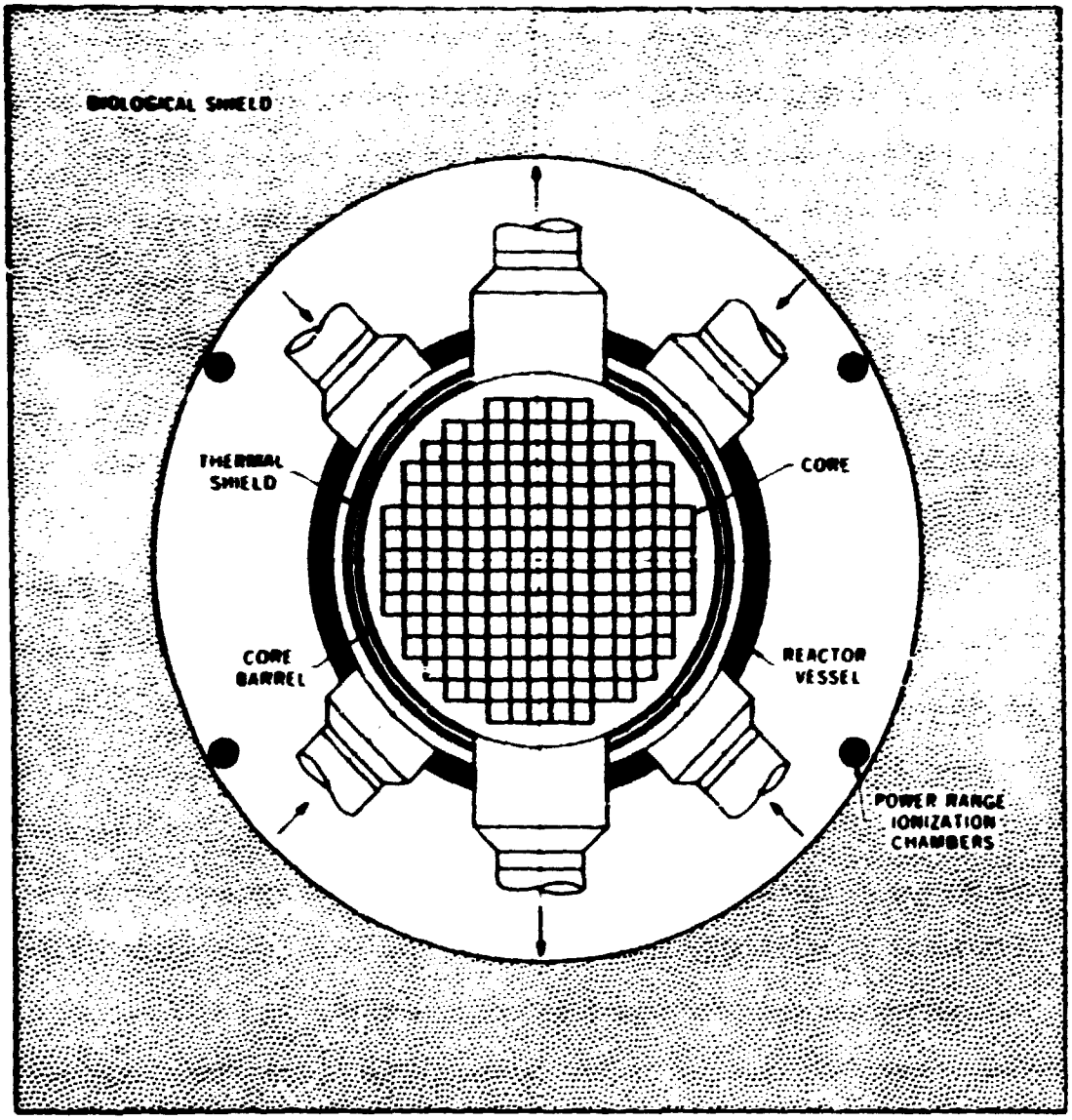

Fig. 2. Cross-sectional view of a typical PWR.

It has been verified experimentally[1] that the core barrel does move at a frequency near its natural resonant frequency, which, typically, is from 4 to 12 Hz. The specific resonant frequency depends on the barrel clamping force and other factors that can vary from unit to unit.

To monitor core barrel motion during normal plant operations, one can statistically analyze (e.g., correlation or spectral density functions) the fluctuating component of signals from ex-core, power-range ionization chambers. These chambers are outside the pressure vessel at the interior biological shield interface, or are slightly inside the biological shield (Fig. 2).

A normally clamped core barrel will move (as will be shown later) a few mils. The response in the ex-core detector signals will be small relative to the mean response (about 10^{-4} relative change in detector response to 1 mil of motion of the core barrel). This relative change will vary with time at a rate (typically, at a few Hertz) determined by the motion of the core barrel. Thus, by utilizing two neutron detectors positioned diametrically across the core from each other and by analyzing the cross-power spectral data from the detectors, one could extract the common component (induced by core motion) from the uncommon components of the fluctuating signals. With this method of statistical analysis, it would not be difficult to measure that part of the detector (ionization chamber) signal which is due to core barrel motion. The amount of core barrel motion could then be determined by applying a scale factor which would convert the detector response to mils of motion. For example, if $\Delta D/D$ represents the fractional detector response induced by core barrel motion and SF the scale factor in units of fractional detector

response per mil, then motion (mils) = (1/SF)(ΔD/D). Furthermore, for the small movements (<500 mils) considered here, SF can be considered a constant, i.e., independent of the actual magnitude of the motion.

4. ANALYTICAL DETERMINATION OF THE SCALE FACTOR

4.1 Scope of the Problem

It is assumed at this point (expanded upon later in this report) that one can extract that portion of the detector response induced by core barrel motion. Thus, the problem is: Given the fraction of the detector response to core barrel motion, what is the motion in mils (0.001 in.) of the core barrel?

The mean displacement of the core barrel is zero; therefore, we are concerned with an oscillatory type of displacement. The time constant characterizing core barrel motion is large (milliseconds) relative to the mean lifetime of the neutrons (microseconds). Hence, even though the problem is inherently a dynamic one, we can assume a quasiequilibrium state for the flux field, i.e., we can use static (steady-state) calculational techniques.

The amount of displacement of the core is necessarily small (there are physical constraints); therefore, the fractional change in detector response will be small. Hence, we must ensure adequate convergence of calculational techniques that rely on differences between large numbers to obtain small numbers.

The power range neutron detectors are often located in air between the pressure vessel and the biological shield. Hence, transport theory must be used since diffusion theory is not applicable in a low-density

medium. The transport model complexity relative to streaming and the geometrical complexity must be verified.

Since the amount of core barrel motion is small, the use of perturbation theory should be considered; remembering, however, that since the actual perturbation is localized, the results obtained using perturbation theory must be demonstrated to be acceptable.

The perturbation is due to changes of the water gap thickness (shield) between the source (reactor core) and the detector. Physically, the movement of the core barrel within the pressure vessel causes the water thickness in the downcomer region to change. Basically, the SF calculation can be treated as a shielding problem, i.e., as a nonmultiplying (no fission) medium with a source (taken to be the mean power density within the core). This procedure reduces the calculation difficulties considerably.

The basic guidelines to be followed in the calculations, if possible, are:

1. use existing transport theory codes,
2. use current cross-section sets that are widely accepted and have been demonstrated to be adequate for shielding calculations,
3. avoid excessive complexity in the transport theory calculations.

4.2 Development of Theoretical Model

The general steady-state neutron transport equation for a critical system is

$$\bar{\Omega} \cdot \nabla \phi(\bar{r},E,\bar{\Omega}) + \sigma(\bar{r},E)\ \phi(\bar{r},E,\bar{\Omega}) =$$

$$\int d\bar{\Omega}' \int dE'\ \sigma_s(\bar{r}',E'\bar{\Omega}'\rightarrow E\bar{\Omega})\ \phi(\bar{r},E',\bar{\Omega}')$$

$$+ \frac{\chi(E)}{4\pi} \int d\Omega' \int dE'\ \nu\,\sigma_f(\bar{r},E',\bar{\Omega}')\ \phi(\bar{r},E',\bar{\Omega}'),$$

where the nomenclature is that used in the literature.[4] For our problem, the power distribution is assumed to be known throughout the core, and we are concerned with finding the flux distribution throughout phase space resulting from this power distribution. Thus, we introduce a source as

$$S(\bar{r},E,\bar{\Omega}) = \frac{\chi(E)}{4\pi} \int d\bar{\Omega}' \int dE' \; \nu \, \sigma_f(\bar{r},E',\bar{\Omega}') \; \phi(\bar{r},E',\bar{\Omega}') \; ,$$

and then solve the nonmultiplying medium problem defined by

$$\bar{\Omega} \cdot \nabla \phi(\bar{r},\ell,\bar{\Omega}) + \sigma(\bar{r},E) \; \phi(\bar{r},E,\bar{\Omega}) =$$

$$\int d\bar{\Omega}' \int dE' \; \sigma_s(\bar{r}',E'\bar{\Omega}' \rightarrow E\bar{\Omega}) \; \phi(\bar{r},E',\bar{\Omega}') + S(\bar{r},E,\bar{\Omega}) \; . \qquad (1)$$

Having the solution to Eq. (1), we can express the effect of interest (reaction rate in the detector) by

$$D = \int_{V_d} d\bar{r} \int dE \int d\bar{\Omega} \; \sigma_d(\bar{r},E) \; \phi(\bar{r},E,\bar{\Omega}) \; . \qquad (2)$$

For simplicity, we introduce an operator $P(\bar{r},E,\bar{\Omega})$ so that Eq. (1) can be written as

$$P \, \phi = S \; , \qquad (3)$$

where the independent variables have been dropped. We proceed by identifying the reference (R) state as the core barrel hanging in its normal position. We identify the operator defined by this state as P_R; then the transport equation for the reference state is written as

$$P_R \, \phi_R = S \; . \qquad (4)$$

The reaction rate in the detector at this reference state is[a]

$$D_R = \langle \sigma_d \phi_R \rangle . \tag{5}$$

Next, we define the perturbed (prime) state to be the core barrel displaced relative to its normal position, and we identify the operator as P' for this perturbed state. Then we write[b]

$$P' \phi' = S \tag{6}$$

and

$$D' = \langle \sigma_d \phi' \rangle . \tag{7}$$

At this point, it is advantageous to introduce a functional F, an importance function ϕ^*, and an adjoint operator P^*. We choose a functional F defined by

$$F = \langle \sigma_d \phi \rangle - \langle \phi^*, P\phi - S \rangle . \tag{8}$$

If the operator P is taken to be P', and ϕ the ϕ' of the perturbed state [Eq. (7)], then F is the expected reaction rate of the detector at the perturbed state. The P^* is taken to be the operator adjoint to P, i.e., P^* is defined by[b]

$$\langle \phi^*, P\phi \rangle = \langle \phi, P^*\phi^* \rangle . \tag{9}$$

---

[a] The symbol < > is used to indicate integration over phase space.

[b] It is assumed that the source (power distribution within the core) is the same for both states.

The importance ϕ^* is the solution to

$$P^* \phi^* = \sigma_d \ . \tag{10}$$

Then an equivalent expression for F is

$$F = \langle \phi^* S \rangle - \langle \phi, P^* \phi^* - \phi_d \rangle \ . \tag{11}$$

Again, if P of Eq. (8) is P′, then P^* would be the adjoint operator corresponding to the perturbed state. Furthermore, ϕ^* [the solution to Eq. (10)] would be the importance function for the detector corresponding to the perturbed state. Obviously, F of Eqs. (8) and (11) are the same; therefore, for the state at which the operators are defined, we have

$$D = F = \langle \sigma_d \phi \rangle = \langle \phi^* S \rangle \ . \tag{12}$$

The scale factor SF is obtained from

$$SF = \frac{|D_1 - D_R|}{D_R} \ , \tag{13}$$

where D_1 is the reaction rate of the detector for a 1-mil displacement of the core barrel, and D_R is the reaction rate at the reference state. As suggested by Eq. (12), there is more than one way to compute SF. In fact, four methods have been pursued herein.

1. forward direct method,
2. adjoint direct method,
3. adjoint difference method,
4. adjoint difference approximate method.

The use of multimethods was considered to be necessary to verify various assumptions which had to be made. The assumptions will be identified at the appropriate place under the discussion of each method.

4.2.1 Forward Direct Method

This is the obvious method, namely, solve the forward transport equation [Eqs. (4) and (6)] for the reference and perturbed fluxes. From this, construct the corresponding detector reaction rate [Eqs. (5) and (7)] and then SF, i.e.,

$$SF = \left|\langle \sigma_d \phi' \rangle - \langle \sigma_d \phi_R \rangle\right| / \langle \sigma_d \phi_R \rangle \ . \qquad (14)$$

The difficulty arises in obtaining the numerator in Eq. (13), which relies on a small difference between nearly equal numbers to obtain a scale factor ($\sim 10^{-3}$ to 10^{-4}) for a 1-mil core barrel motion. Accordingly, the transport equations must be solved to a high degree of accuracy on the flux (tight convergence criteria) if the numerator of Eq. (14) is to be significant. In fact, we found it impractical to estimate SF from Eq. (14) for only 1-mil core barrel displacement. The procedure we were forced to adopt was to solve the transport equation for a larger core barrel displacement (100 mils was the lower practical limit) and then to assume that SF (on a per mil basis) is independent of displacement by dividing the result of Eq. (14) by the core displacement actually used.

To establish confidence in the SF values calculated using the forward direct method, we must assure convergence of the solution to the transport equation and verify the assumption that SF (on a per mil basis) is independent of displacement. Convergence was assured by (a) changing the convergence criteria, (b) changing mesh spacing, and (c) calculating SF

using alternative formulas (described below). The assumption that the SF is essentially independent of displacement up to 500 mils was checked using alternative formulas.

4.2.2 Adjoint Direct Method

This method requires solution of the adjoint equations

$$P_R^* \phi_R^* = \sigma_a \ , \tag{15}$$

and

$$P^{*\prime} \phi^{*\prime} = \sigma_d \ .$$

where P_R^* is the adjoint operator for the reference state, and $P^{*\prime}$ is the adjoint operator for the perturbed state. The SF is constructed from

$$SF = \frac{|\langle \phi^{*\prime} S \rangle - \langle \phi_R^* S \rangle|}{A \langle \phi_R^* S \rangle} \ , \tag{16}$$

where A is the number of mils the core barrel is displaced in the perturbed state relative to the reference state.

The primary objectives of the adjoint direct method are (a) to establish confidence in the adequate convergence of the various methods through redundancy, and (b) to obtain the importance functions for use in the adjoint difference method and adjoint difference approximate method.

4.2.3 Adjoint Difference Method

We introduce a difference flux $\delta\phi$ as

$$\delta\phi \equiv \phi^{\prime} - \phi_R \ , \tag{17}$$

and a difference operator as

$$\delta P = P' - P_R \ . \tag{18}$$

To obtain the transport equation for the difference flux, we postulate that ϕ_R and δP are known. Then we subtract the reference forward equation [Eq. (4)] from the perturbed forward equation [Eq. (6)]. The result is

$$P' \, \delta\phi = Q \ , \tag{19}$$

where Q is a source term constructed from

$$Q = - \delta P \, \phi_R \ . \tag{20}$$

Of course, SF can then be constructed from

$$SF = \langle \sigma_d \, \delta\phi \rangle / (A \langle \sigma_d \, \phi_R \rangle) \ , \tag{21}$$

where A is the same as in Eq. (16).

Since the source Q in Eq. (20) can be positive and negative, some difficulty may be experienced in numerically obtaining $\delta\phi$; therefore, we consider an alternative calculation. We introduce the functional δF as

$$\delta F \equiv \langle \sigma_d \, \delta\phi \rangle - \langle \phi^*, \, P\delta\phi - Q \rangle \ . \tag{22}$$

An equivalent expression for δF is

$$\delta F = \langle Q \, \phi^* \rangle - \langle \delta\phi, \, P^* \, \phi^* - \sigma_d \rangle \ . \tag{23}$$

If we choose P to be P′ and $\delta\phi$ to be the solution to Eq. (19), then δF of Eq. (22) is the numerator of Eq. (21). Correspondingly, we choose P* of Eq. (23) to be P*′ and ϕ^* to be the solution to

$$P^{*\prime}\ \phi^{*\prime} = \sigma_d \ . \tag{24}$$

Then SF can be obtained from

$$SF = \frac{|\langle Q\ \phi^{*\prime}\rangle|}{A\langle\sigma_d\ \phi_R\rangle} = \frac{|\langle Q\ \phi^{*\prime}\rangle|}{A\langle S\ \phi_R^*\rangle} \ . \tag{25}$$

Equation (25) is the adjoint difference method for computation of SF. The adjoint function $\phi^{*\prime}$ of Eq. (24) is the same function as that used in the previous methods, i.e., it is the solution to the perturbed state importance (or adjoint) equation.

The advantage of using the adjoint difference method relative to the previously discussed methods is that one is not required to take the difference in computed state variables (ϕ' and ϕ_R). Therefore, the convergence requirements are expected to be somewhat less.

4.2.4 Adjoint Difference Approximate Method

For this method, we expand the importance function for the perturbed state [solution to Eq. (24)] to

$$\phi^{*\prime} = \phi_R^* + \delta\phi^* \ , \tag{26}$$

where ϕ_R^* is the solution to the importance equation at the reference state, i.e., the solution to

$$P_R^*\ \phi_R^* = \sigma_d \ . \tag{27}$$

We substitute Eq. (26) into Eq. (25) and ignore second-order terms (Q itself is first order) to obtain

$$SF = \frac{|\langle Q\ \phi_R^* \rangle|}{A\langle \sigma_d\ \phi_R \rangle} . \tag{28}$$

Equation (28) is equivalent to linear perturbation theory.[5]

The variables in Eq. (28), that is, the ϕ_R (in Q) and ϕ_R^*, are solutions to the reference state equations. Since the perturbed state appears only in the operator term δP, any size of perturbation can be considered in the solution to this equation. In particular, the assumption employed in the direct methods that the SF is independent of the core barrel displacement can be checked by employing the adjoint difference approximate method.

4.3 Calculational Model

The problem is to compute the reaction rate in the ex-core ionization chambers (Fig. 2) for the conditions of the core barrel in both its reference position and a slightly displaced position. The reactor is assumed to be operating at constant power with a known power distribution. The core barrel will move inside the pressure vessel, varying the thickness of water in the annulus between the core barrel and the pressure vessel and, therefore, the amount of shielding between the core (source) and the ex-core ionization chamber.

To explicitly model the geometric complexity of the core barrel displaced relative to its center would require excessive computation time; therefore, we chose to simulate core barrel displacement by varying the

density of the water between the core barrel and the pressure vessel (this is mathematically equivalent if the density is varied such that the number of mean free paths traversed by the neutrons is the same as would be the case if the core barrel were actually displaced).

The power distribution (spatial source distribution) used for the calculations was taken to be that of a typical PWR (reproduced in the Appendix, Fig. 12). The energy distribution of the source was assumed to be the fission spectrum. The solutions to the neutron transport equations were obtained using multigroup discrete ordinates[4] codes, in particular, ANISN[6] and DOT[7] for one-dimensional and for two-dimensional calculations, respectively. The reference (standard) cross-section set used was a P-1, 22-neutron--18-gamma group coupled set[8] obtained from the Radiation Safety Information Center (RSIC) at the Oak Ridge National Laboratory. An alternative set of cross sections was used for verification purposes, the 16-group Hansen and Roach[9] set originated by the Los Alamos Scientific Laboratory and distributed by RSIC. The angular quadrature set corresponded to an S_4 calculation in both the one-dimensional (cylindrical) and two-dimensional (R-θ) geometries. Calculations were made to check the adequacy of these quadrature sets: S_{16} calculations in the one-dimensional and S_6 calculations in the two-dimensional geometries.

Figure 3 is a diagram of the one-dimensional (cylindrical geometry) model. The materials used in each zone, the number densities, and the mesh spacing are listed in the Appendix, Table 5. The amount of biological shield in the model was chosen to be 3-4 neutron migration lengths because this adequately represents an infinite shield. The source for

the forward calculations was distributed throughout the core zone. The source for the adjoint calculation was at the air-biological shield interface. A vacuum boundary condition was employed at the outer edge of the biological shield.

Figure 4 is a diagram of the two-dimensional model. The materials in each zone and radial mesh spacing were the same as used in the one-dimensional model. Sixty equal $\Delta\theta$ spacings were used in the half-cylinder shown in Fig. 4. Vacuum boundary conditions were used at the outer edge of the biological shield, and symmetric boundary conditions were employed about the diameter.

The core barrel displacement was simulated as follows:

1. In the one-dimensional model, the density of the water in the gap between the thermal shield and reactor vessel was changed to simulate an expansion (or contraction) of the entire core barrel.

2. In the two-dimensional model, the density of the water between the thermal shield and reactor vessel in each $\Delta\theta$ segment was changed proportionately to simulate a simple displacement of the core barrel in the X-direction. The source for the two-dimensional adjoint calculation was located at the air-biological shield interface at an angle θ of 60°, measured counterclockwise from the X-direction.

4.4 Results of Analytical Determination of SF

Unless otherwise indicated, all results presented herein were obtained using

1. the 22 neutron--18 gamma cross-section set described in ref. 8,

ORNL-DWG 76-7811R

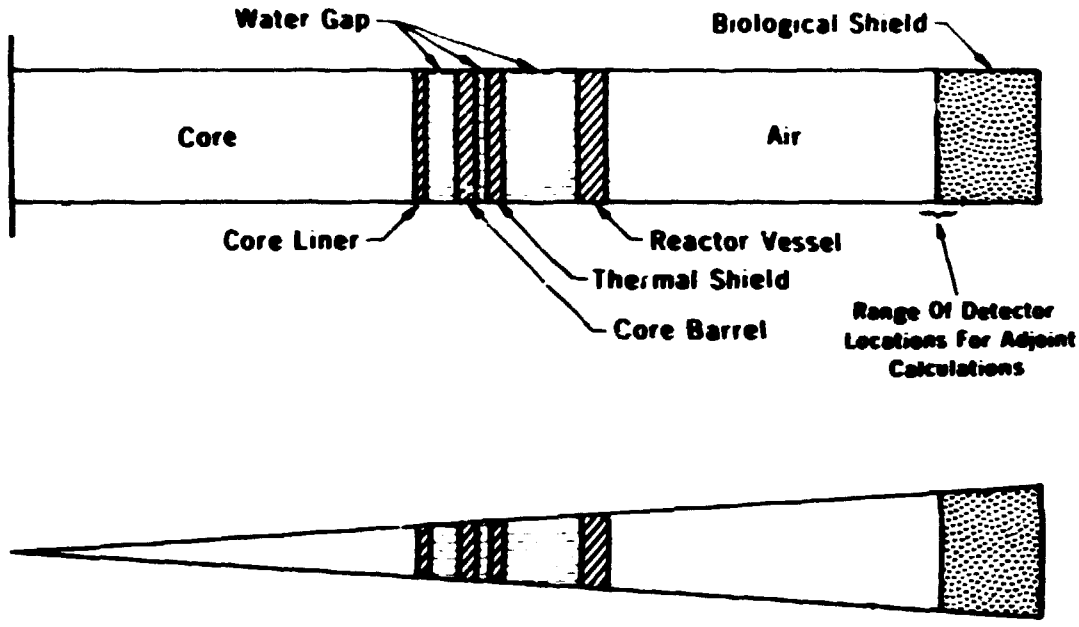

Fig. 3. One-dimensional model (cylindrical geometry).

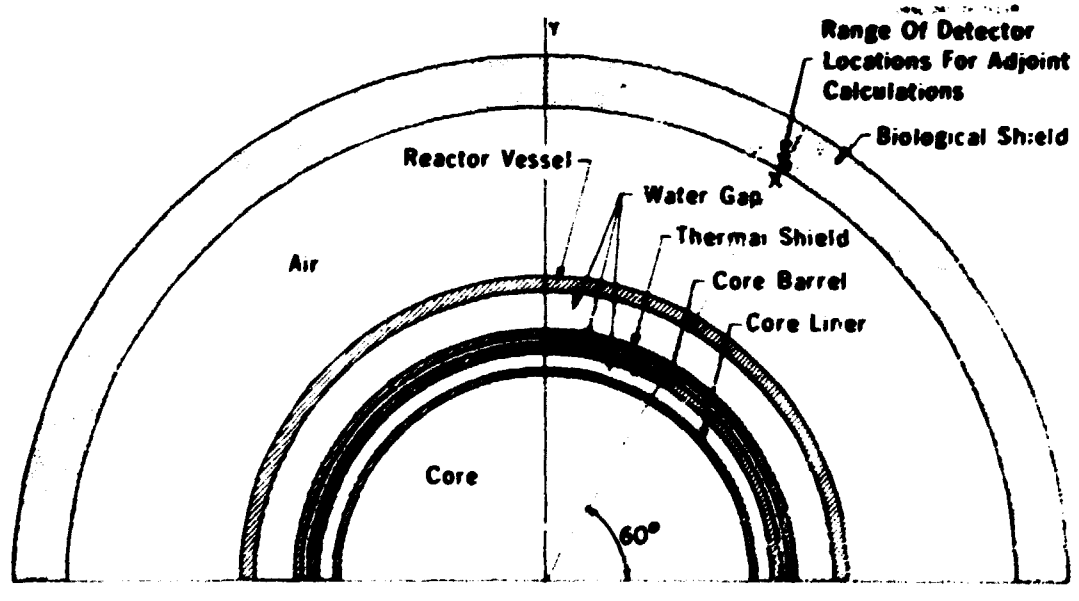

Fig. 4. Two-dimensional (R-θ) model.

2. an S_4 quadrature set with P-1 scattering,
3. cylindrical geometry for the one-dimensional calculations and R-θ geometry for the two-dimensional calculations.

The results for the one-dimensional calculations will be presented first, followed by results from the two-dimensional analysis and, finally, by conclusions and recommendations relative to the analytical results.

4.4.1 Results from One-Dimensional Analysis

The solution to the appropriate transport equation (ϕ_R, ϕ', ϕ_R^*, or $\phi^{*\prime}$) was computed using the discrete ordinates code ANISN[6] and stored on tape for further processing. The equation to be solved in each method is the following.

1. Forward Direct Method:

$$SF = \frac{|\langle \sigma_d \phi' \rangle - \langle \sigma_d \phi_R \rangle|}{A \langle \sigma_d \phi_R \rangle}, \tag{29}$$

where A is the core barrel displacement in mils used for the perturbed state.

2. Adjoint Direct Method:

$$SF = \frac{|\langle \phi^{*\prime} S \rangle - \langle \phi_R^* S \rangle|}{A \langle \phi_R^* S \rangle}, \tag{30}$$

where S is the source used for the forward transport equation.

3. Adjoint Difference Method:

$$SF = \frac{|\langle Q\ \phi^{*'}\rangle|}{A\ \langle \sigma_d\ \phi_R\rangle}\ , \tag{31}$$

where Q is defined previously (Eq. 20).

4. Adjoint Difference Approximate Method:

$$SF = \frac{|\langle Q\ \phi_R^{*}\rangle|}{A\ \langle \sigma_d\ \phi_R\rangle}\ . \tag{32}$$

The phase space integrals in the forward direct and adjoint direct methods are straightforward; hence, a simple program was written to carry out those integrals. The integrals in the adjoint difference and the adjoint difference approximate methods are somewhat more difficult, i.e.,

$$|\langle Q\ \phi^{*}\rangle| = |\langle \phi^{*}\ \delta P\ \phi_R\rangle|\ . \tag{33}$$

Since the integral in Eq. (33) is the same type as carried out by the SWANLAKE[10] code, this code was used for the adjoint difference and the adjoint difference approximate calculations.

The results obtained by the four methods are listed in Table 1. The forward direct, adjoint direct, and adjoint difference methods all were calculated using a core barrel displacement of 500 mils (that is, by changing the water gap number density, the outer radius of the thermal shield was allowed to "expand" 500 mils), with the assumption that the difference in detector response is linear with the core barrel displacement so that the SF could be expressed on a "per mil" basis. The results

obtained by the adjoint difference approximate method were computed for the same 500 mil displacement. Owing to its formulation as an expansion about the reference state, an assumption of linearity is inherent in this method. From the close agreement of the results of this latter method with the other methods, we conclude that the linear approximation is valid, at least for one-dimensional analysis.

Table 1. Analytical scale factor from one-dimensional analysis

Method	Scale Factor, SF (% per mil)
Forward Direct	0.041
Adjoint Direct	0.041
Adjoint Difference	0.040
Adjoint Difference Approximate	0.038

Many variations were made in the one-dimensional analysis. The important variations and conclusions are:

1. The SF was calculated with and without the effects of gammas, but there was no observable effect due to gammas; therefore, gammas can be ignored in two-dimensional cases (this reduces the total number of groups from 40 to 22).
2. Values of SF were calculated by changing the angular quadrature from S_4 to S_{16}. The higher angular quadrature set had no effect on the SF, so we conclude that S_4 is adequate.

3. The core barrel displacement was reduced from 500 to 100 mils. The convergence requirements on the solutions to the forward and adjoint equations were stiffer, but the calculated SFs were essentially the same as those in Table 1. It was obvious that core barrel displacement much less than 100 mils would be very expensive to analyze because of the stringent convergence requirements on the solution to the transport (forward and adjoint) equations.
4. The Hansen and Roach 16-neutron group, P-1 cross-section set[9] replaced the shielding 22-neutron--18-gamma group coupled set. In general, the results for the SF with the 16-group set were 5 to 10% greater than the results in Table 1. We chose to use the results from the 22-neutron--18-gamma group set because (a) the latter is a more recent set and was developed specifically for shielding calculations, and (b) the lower value of the SF is more conservative relative to estimating an upper limit of core barrel motion from spectral density measurements (illustrated in the next section).
5. The amount of boron in the water was varied to simulate core burnup conditions. This had no significant effect on the SF.

4.4.2 Results from Two-Dimensional Analysis

The methods for this analysis are the same four that were used for one-dimensional analysis. The values of the SF calculated for an ex-core detector at 60° and a maximum displacement of 500 mils are listed in Table 2. The two-dimensional (R-θ geometry) transport equations were solved using DOT:[7] (1) a flux tape was obtained from DOT; (2) a code was written to evaluate the integrals of Eqs. (29) and (30); and (3) the numerators of Eqs. (31) and (32) were calculated again using SWANLAKE,

but an intermediate code VIP[11] was required to couple the DOT output with SHAKLAKE.

The source for the adjoint equation (detector) was arbitrarily chosen to be at an angle θ of 60° relative to the diameter along which the maximum core barrel displacement occurs (the X-direction). The mil unit used in computing the SF (i.e., SF in percent per mil) refers to the maximum displacement of the core barrel in this X-direction. Therefore, the SF is dependent on the angle θ at which the detector is located and will be a maximum at 0°. However, it is to be expected that the maximum SF for the two-dimensional case (0.016% per mil from Table 2) will be less than that for the one-dimensional case (0.040% per mil from Table 1), since the total geometrical perturbation induced is not as large in two dimensions. This is true because we must allow the entire core barrel to expand as a cylinder in the one-dimensional analysis, whereas the two-dimensional analysis allows us to simulate the core barrel displacement more realistically. In particular, if the water gap thickness between the reactor core and an ex-core detector at one side of the core is reduced, there must realistically be a corresponding increase in the water gap thickness between the core and an ex-core detector at the opposite side of the core, and two-dimensional analysis allows this requirement to be met.

The results in Table 2 also show a larger discrepancy between the SF calculated by the adjoint difference approximate method and the SFs calculated in two dimensions by the other methods than is shown in Table 1 for one-dimensional analysis. This suggests that the assumption of linearity is less valid for two-dimensional analysis than for one-dimensional analysis, which seems plausible. Of the values in Table 2,

we have greatest confidence in those calculated by the forward direct and the adjoint difference approximate methods because they have the tightest convergence. For small displacements (a few mils), we believe the 0.0095 (~0.01) value in Table 2 is probably the more correct because the "per mil" value from the forward direct method was obtained by assuming that the SF is independent of displacement up to 500 mils, whereas the adjoint difference approximate method is constructed as an expansion about the reference state and thus is inherently most accurate for small displacements.

Table 2. Analytical scale factor from two-dimensional analysis

Method	Scale Factor, SF (% per mil) with Ex-Core Detector[a]	
	at 0°	at 60°
Forward Direct	0.016	0.0075
Adjoint Direct	--	0.0083
Adjoint Difference	--	0.0072
Adjoint Difference Approximate	--	0.0095

[a]The location of the ex-core detector was measured at an angle relative to maximum core barrel displacement. Zero degrees is along the direction of maximum displacement. The detector is taken to be in the air at the inner boundary of the biological shield (Fig. 2).

The SF calculated by the forward direct method as a function of angle relative to the assumed direction of core barrel displacement is presented in Fig. 5. The shaded area shows the dependence of SF on the physical location of the detector (see also Fig. 4), i.e., a location slightly inside the biological shield (a design favored by some manufacturers) produces a greater SF than one at the inner air-biological shield interface. From Fig. 5, we can conclude that the SF for a detector located at 90° relative to the direction of motion is quite small (approaching, but not equal to, zero). Thus, once the preferred direction of motion (which can be established either from ex-core detector spectral data or from the physical layout of the core barrel, inlet and exit coolant pipes) is established, it is advantageous to choose ex-core detectors that are as nearly parallel to the preferred direction of motion as possible.

To assure the accuracy of the two-dimensional results, we took considerable care in our calculations. The more significant steps were:

1. The order of the discrete ordinates approximation was verified by repeating the analysis using an S_6 quadrature set generated by Simpson[12] for R-θ geometry. There was no significant change in results over the conventional S_4 set used for the normal calculations.
2. Mesh spacing in both the R and θ directions was varied around the detector, but this produced no significant change in the SF.
3. The DOT-VIP-SWANLAKE combination was applied to the one-dimensional cylindrical problem solved previously with ANISN-SWANLAKE. The SF values calculated using DOT-VIP-SWANLAKE were the same as those from ANISN-SWANLAKE for this one-dimensional case. This gave us further

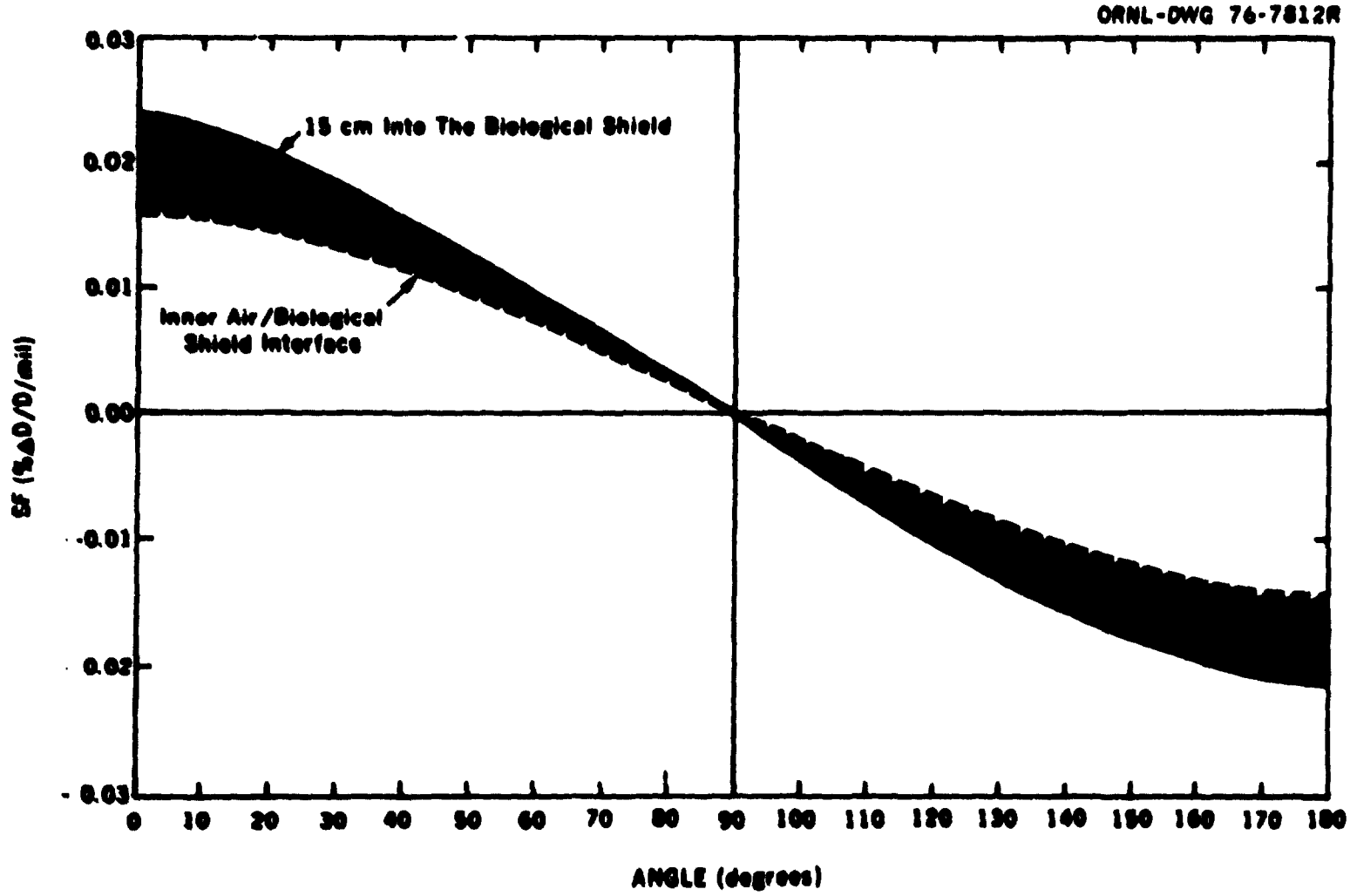

Fig. 5. Results from computations using the two-dimensional model and DOT R-θ.

confidence in the correctness of our two-dimensional calculational procedures.

4.4.3 Conclusions and Recommendations Relative to the Analytical Results

From the results obtained by one- and two-dimensional analysis, we draw the following general conclusions:

1. The practice of computing the SF using one-dimensional analysis and then assuming a "cosine" magnitude variation with the angular rotation of the detectors relative to the preferred direction of displacement is erroneous. The major problem is that the detector in the air at the air-biological shield interface is affected by radiation streaming out in regions where there is little perturbation; this radiation is scattered to the detector (the problem is analogous to "skyshine" in shadow shielding a target).
2. The forward direct method is applicable to the calculation of the SF. To do this the core barrel must, because of calculational difficulties, be displaced 100 to 500 mils; the SF is computed by assuming that it is essentially independent of displacement. The results are acceptable.
3. The adjoint difference approximate method is acceptable and easily applied once the forward and adjoint functions characteristic of the reference state are available.

Our recommendation is to use the forward direct method as a shielding calculation for a core barrel displacement of 400 or 500 mils; however, care should be taken to assure convergence. Since we have not explored the use of diffusion theory and the nature of the problem does

not lend itself to the assumptions of diffusion theory, we cannot recommend its use. We conclude that the cross-section set (the P-1, 22-neutron group--18-gamma group coupled set obtained from RSIC) used in this work is adequate; however, we cannot recommend that an angular approximation of less than S_4 be used, because we did not test such.

5. DETERMINATION OF CORE BARREL MOTION

In this section we illustrate the determination of core barrel motion in mils using statistical descriptors and the SF. The reader is referred to refs. 13-16 for detailed discussions of the various statistical descriptors and the methods of obtaining them. This section begins with a minimal discussion of these descriptors to clarify their use for the determination of core barrel motion. After this discussion, the application is described, using experimental data.

5.1 Statistical Descriptors for Core Barrel Motion Determination

Electric current signals from ex-core ionization chambers with the reactor at steady state power have been used to determine core barrel motion. The signals have a steady state (mean) value $\bar{I}$ with a fluctuating component δI about the mean, i.e.,

$$I(t) = \bar{I} + \delta I(t) \ . \tag{34}$$

The fluctuating component is produced by several driving functions, such as reactivity fluctuations that cause power fluctuations, statistical fluctuations of the reaction rate within the detector, and neutron transmittance variations between the core and detector due to core barrel motion. Because each fluctuating component is small, the system behaves

as a linear system, and the principle of superposition is valid. The objective is to separate a component of interest (the component due to core barrel motion) from the other components or else to demonstrate that the other components can be safely ignored.

The statistical descriptors for our purpose are the cross- and auto-power spectral densities and the amplitude probability density function. Although, formally, spectral density functions can be defined as the Fourier transform of the correlation functions,[13] it is convenient for our purposes to construct the spectral density functions directly in the frequency domain (the equivalence of two different methods for construction of the spectral density function is proved in ref. 13).

We denote the fluctuating component of the signal from detector 1 as

$$\delta I_1(t) = \delta I_{1c}(t) + \delta I_{1\rho}(t) + \delta I_{1D}(t) , \tag{35}$$

where δI_{1c} is the component of the detector signal induced by core barrel motion, $\delta I_{1\rho}$ is the component due to reactivity fluctuation, and δI_{1D} is the fluctuation component due to statistical variations of the reaction rate within the detector. Similarly for detector 2, we write

$$\delta I_2(t) = \delta I_{2c}(t) + \delta I_{2\rho}(t) + \delta I_{2D}(t) . \tag{36}$$

We obtain a record (an ensemble) of the fluctuating components of the signal from each detector for a period of time T, then Fourier transform each ensemble, and form the product[7] $\delta I_1^*(f)\, \delta I_2(f)$, i.e.,

---

[7]The superscript * signifies complex conjugate.

$$\delta I_1^*(f)\,\delta I_2(f) = \delta I_{1c}^*(f)\,\delta I_{2c}(f) + \delta I_{1c}^*(f)\,\delta I_{2\rho}(f)$$

$$+ \delta I_{1c}^*(f)\,\delta I_{2D}(f) + \delta I_{1\rho}^*(f)\,\delta I_{2c}(f) + \delta I_{1\rho}^*(f)\,\delta I_{2\rho}(f)$$

$$+ \delta I_{1\rho}^*(f)\,\delta I_{2D}(f) + \delta I_{1D}^*(f)\,\delta I_{2c}(f)$$

$$+ \delta I_{1D}^*(f)\,\delta I_{2\rho}(f) + \delta I_{1D}^*(f)\,\delta I_{2D}(f)\ . \qquad (36)$$

The procedure is to take many ensembles (say N records, each of length T), Fourier transform each, form the conjugate cross product, and then determine the average (ensemble average) of the cross products. The result will be the power spectral density (PSD) if detectors 1 and 2 are physically the same detector:

$$PSD_1(f) = \langle \delta I_1^*(f)\,\delta I_1(f)\rangle = \langle \delta I_{1c}^*(f)\,\delta I_{1c}(f)\rangle$$

$$+ \langle \delta I_{1\rho}^*(f)\,\delta I_{1\rho}(f)\rangle + \langle \delta I_{1D}^*(f)\,\delta I_{1D}(f)\rangle\ . \qquad (37)$$

The result will be the cross-power spectral density (CPSD) if the detectors are different:

$$CPSD_{12}(f) = \langle \delta I_1^*(f)\,\delta I_2(f)\rangle = \langle \delta I_{1c}^*(f)\,\delta I_{2c}(f)\rangle$$

$$+ \langle \delta I_{1\rho}^*(f)\,\delta I_{2\rho}(f)\rangle\ , \qquad (38)$$

where $\langle\ \rangle$ represents the ensemble average. The cross terms in Eq. (37) [relative to Eq. (36)] are missing since those terms are statistically independent and hence their ensembles average to zero in

the limit. The last term in Eq. (37) is missing in Eq. (38) because the statistical fluctuations in the reaction rates of the different detectors are uncorrelated.

The terms that make up Eq. (35) were not intended to be all inclusive. Therefore, there may be more terms than shown in Eq. (37); however, even if there were additional terms they would still not appear in Eq. (38) unless the fluctuations appearing in the detector signals originated from a common source. They would appear in Eq. (37), however, since the mean square of that fluctuating component would not be zero. On this basis, it is instructive to consider the coherence $\gamma^2(f)$ given by

$$\gamma^2(f) = \frac{|CPSD_{12}(f)|^2}{PSD_1(f)\ PSD_2(f)} \quad . \tag{39}$$

From Eqs. (37) and (38), it is obvious that $\gamma^2(f)$ is bounded between zero (no correlation between the two detectors) and unity (perfect correlation between the fluctuating signals received by the two detectors). Therefore, if there is a frequency range where most of the signals seen by the two detectors are induced by a common cause (barrel motion), the coherence will be significant over that frequency range. Hence, the coherence is a key statistical parameter in identifying the component of interest in the detector signal, i.e., the component induced by core barrel motion [see Eq. (35)].

In addition to the coherence, the phase $\phi(f)$ associated with the $CPSD_{12}(f)$ is also useful in identifying that component of the detector signal induced by core barrel motion. To establish this, we assume that the ex-core detectors are located on opposite sides of the reactor core.

Thus, whenever the reactor core moves toward detector 1, it moves away from detector 2. Symbolically, we represent this as

$$S(f) + \delta T_1(f) + \delta I_1(f)$$

and

$$S(f) + \delta T_2(f) - \delta I_2(f) \ ,$$

where S represents the varying reactor source, and δT represents the varying neutron transmittance from the core to the detector output. We write the deviation in transmittance $\delta T_1(f)$ as

$$\delta T_1(f) = \delta A(f)\ e^{j\phi_1} \ ; \tag{40}$$

then $\delta T_2(f)$ (which differs only in phase by π radians) can be written as

$$\delta T_2(f) = \delta A(f)\ e^{j(\phi_1 - \pi)} \ . \tag{41}$$

Finally, the component of the CPSD due to core barrel motion is

$$\begin{aligned} CPSD_{12}(f) &= \langle \delta I^{*}_{1c}(f)\ \delta I_{2c}(f) \rangle \\ &= S^2 \langle |\delta A(f)|^2 \rangle\ e^{-j\pi} \ . \end{aligned} \tag{42}$$

Hence, the phase of the component of the CPSD (for two detectors positioned on opposite sides of the core and influenced by movement of the core barrel in a pendulum-mode motion) will be 180°.[3] In contrast to

---

[3]Higher-mode vibrations can lead to components in the CPSD with 0° phase, but these will occur at higher frequencies than the pendulum-mode vibrations.

this, reactivity perturbations will generally lead to components in the CPSD that are in phase (i.e., the total power will go either up or down simultaneously across the entire core).

In summary, we use the coherence and phase of the $CPSD_{12}(f)$ to identify that frequency range over which the component of the $CPSD_{12}(f)$ attributable to core barrel motion is dominant. Once we have separated out the core barrel motion component, we proceed to quantify the motion, as discussed below.

It is useful at this point to consider an alternative formulation of the cross-spectral density function, i.e., the cross-power spectral density computed from the Fourier transform of the cross-correlation function $C_{12}(\tau)$, where

$$C_{12}(\tau) = \lim_{T\to\infty} \frac{1}{T} \int_{-T/2}^{T/2} \delta I_1(t+\tau)\, \delta I_2(t)\, dt \ . \tag{43}$$

Thus

$$CPSD_{12}(f) = \int_{-\infty}^{+\infty} C_{12}(\tau)\, e^{-2\pi j f \tau}\, d\tau \ . \tag{44}$$

From Eq. (43), we note that the variance between detectors 1 and 2 is given by the cross-correlation function at zero lag, i.e.,

$$\sigma_{12}^2 = C_{12}(0) \ . \tag{45}$$

Hence,

$$\sigma_{12}^2 = \int_{-\infty}^{+\infty} CPSD_{12}(f)\, df \ , \tag{45}$$

from Eq. (44). Moreover, if we assume that we have isolated, by careful selection of the frequency band $f_U - f_L$ over which core barrel motion is dominant, that portion of the CPSD which is induced by core barrel motion; then the RMS value of core barrel motion is given by

$$\text{RMS} = \left[\int_{f_L}^{f_U} \text{CPSD}_{12}(f)\, df \right]^{1/2} . \tag{46}$$

To obtain motion in absolute units, it is convenient to use the normalized cross-power spectral density $\text{NCPSD}_{12}(f)$ given by

$$\text{NCPSD}_{12}(f) = \frac{\langle \delta I_1^*(f)\, \delta I_2(f) \rangle}{\bar{I}_1\, \bar{I}_2} , \tag{47}$$

which has the dimension of frequency^{-1}. For the case of the component of the CPSD produced by core barrel motion [using Eqs. (40) and (41)],

$$\text{NCPSD}_{12}(f) = \frac{\langle \delta T_1^*(f)\, \delta T_2(f) \rangle}{\bar{T}_1\, \bar{T}_2} , \tag{48}$$

where δT_1 and δT_2 are the deviations in transmittance about their respective means $\bar{T}_1$ and $\bar{T}_2$ for detectors 1 and 2, respectively. Thus, the RMS value of motion (in mils) is obtained from

$$\text{RMS}\Big|_{\text{mils}} = \frac{100}{SF} \left[\int_{f_L}^{f_U} \text{NCPSD}_{12}(f)\, df \right]^{1/2} , \tag{49}$$

where SF is expressed in % per mil as described in the preceding section.

As a final observation, we note that the RMS value given by Eq. (49) represents one standard deviation of motion if we assume[a] that the motion obeys gaussian statistics. Making this assumption, we can proceed to establish a priori RMS limits such that the probability that the peak motion will exceed some specified amount is arbitrarily small. For example, the probability that the peak motion will exceed ±1 standard deviation (crest factor = 1.0) is ~0.32, while the probability that the peak motion will exceed ±1.96 standard deviations is ~0.05. Thus, we introduce a "crest factor," by which we multiply the RMS value to obtain a peak value; we are confident (at a specified confidence level) that with the given RMS value the peak motion will not exceed this peak value. Such crest factors (obtained from probability tables) are presented in Table 3 (p. 38).

5.2 Application of the Experimental Statistical Descriptors to Determination of Core Barrel Motion[b]

To verify core barrel motion, we first identify the dominant frequency range in which the motion may be occurring and then demonstrate that we can distinguish the core barrel motion signal from the remaining fluctuating components of the signal. We have two ex-core ionization

---

[a]The statistical distribution function describing the amplitude of the actual motion can be established from the experimentally observed amplitude probability density functions (APDs), as will be demonstrated in Sect. 5.2.

[b]The experimental data presented in this section were chosen to be generally representative of PWRs.

chambers diametrically opposite each other. For the fluctuating components of these detector signals, we construct normalized power spectral densities NPSD(f), i.e.,

$$NPSD_i(f) = \frac{\langle \delta I_i^*(f)\ \delta I_i(f) \rangle}{\bar{I}_i^2} , \tag{50}$$

where subscript i refers to the ith detector (1 or 2). The NCPSD(f) is given by

$$NCPSD_{12}(f) = \frac{\langle \delta I_1^*(f)\ \delta I_2(f) \rangle}{\bar{I}_1\ \bar{I}_2} , \tag{51}$$

and the coherence $\gamma^2(f)$ by

$$\gamma^2(f) = \frac{|NCPSD_{12}(f)|^2}{NPSD_1(f)\ NPSD_2(f)} , \tag{52}$$

and the phase by

$$\theta = \tan^{-1} \left\{ \frac{Im[NCPSD_{12}(f)]}{Re[NCPSD_{12}(f)]} \right\} . \tag{53}$$

In Fig. 6, there is high coherence in the 7- to 12-Hz frequency range. In Fig. 7, the phase is -180° in this range of high coherence. Hence, we conclude that there is pendulum-mode core barrel motion in this frequency range.

The next step is to determine the amount of core barrel motion, as follows. We obtain the RMS value for motion in accordance with Eq. (49). Figure 8 is a plot of the $|NCPSD_{12}(f)|$ for a frequency range of 2 to 20 Hz; this frequency band is actually greater than the 7- to 12-Hz range

suggested by the coherence and phase for pendulum-mode motion, but the dominant part of the $|MCPSD_{12}(f)|$ largely coincides with the pendulum-mode motion frequency. Using Eq. (49), an SF value from Fig. 5 of 0.01% mil^{-1}, and the data in Fig. 8, we calculate an RMS value of 1.5 mils motion. Assuming a crest factor of 4, we would not expect any more than three or so "peak motions" per hour to exceed ±6.0 mils (Table 3) if we have near-gaussian motion.

Table 3. Crest factors assuming gaussian statistics

Confidence Level (%)	Crest Factor	Expected Number[a] of Times Peak Motion Will Exceed Specified RMS Limit (hr^{-1})
68.2	1.0	11,400
95	1.96	1,800
99	2.6	360
99.9	3.3	36
99.95	3.4	18
99.99	3.9	3.6
99.999	4.4	0.4
---	5.0	0.02

[a]Expected number of times peak motion will exceed RMS motion is based on an assumed (but typical) nominal frequency of 10 Hz for the core barrel motion, i.e., a challenge rate of 3.6×10^4 hr^{-1} .

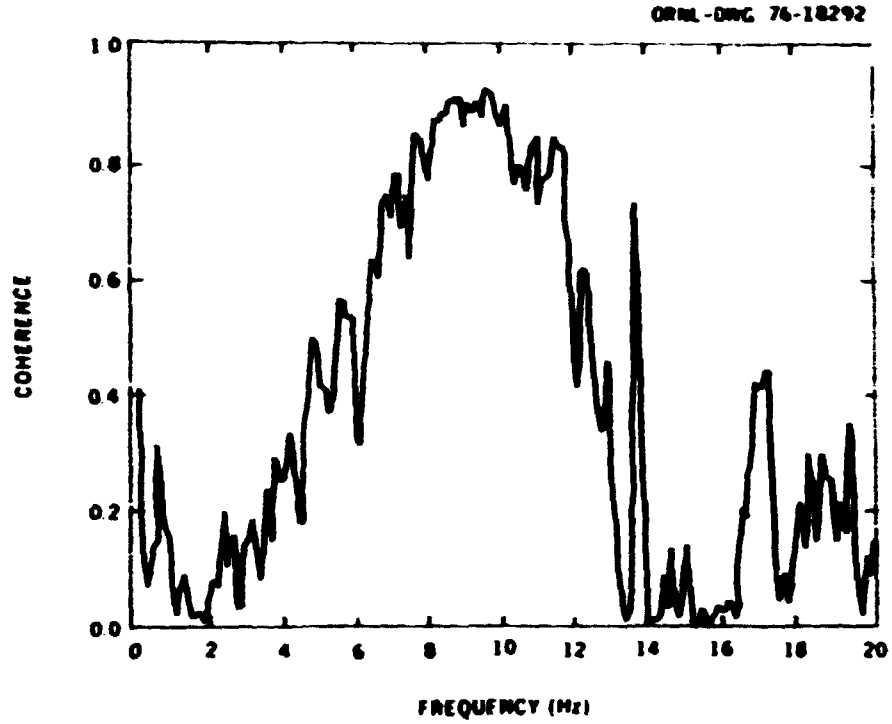

Fig. 6. Coherence vs frequency (frequencies <2 Hz suppressed).

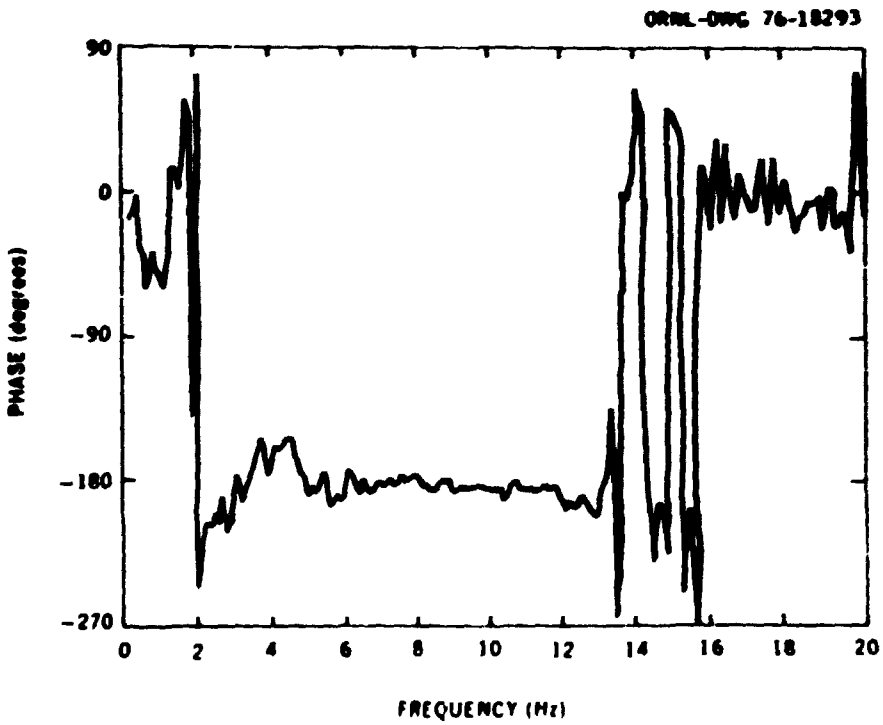

Fig. 7. Phase vs frequency (frequencies <2 Hz suppressed).

To explore the hypothesis that the pendulum-mode displacement is described by gaussian statistics, an APD function is constructed first for the raw time signal and then for a band-limited time signal.

Before it is converted from an analog to a digital signal, the raw time signal is band limited for frequencies >0.01 Hz (by the ac amplifier used in data acquisition) and <25 Hz (by an antialiasing filter). The APD function of the resultant broad-band (0.01 to 25.0 Hz) signal plotted in Fig. 9 in no way resembles a gaussian distribution function, which was assumed to obtain the crest factors in Table 3. In fact, if we were to attribute the abscissa extrema of Fig. 9 to pendulum-mode motion, we would be led to the conclusion that the core barrel sometimes moves as much as 46 mils, a ridiculous value since it is larger than the clearance between the core barrel and the lower snubbers. Obviously, the time trace signal from which Fig. 9 was constructed contains a sinusoidal component; since this is not apparent in the $|NCPSD_{12}(f)|$ data of Fig. 8, its frequency must be less than 2 Hz. An analysis at lower frequencies showed the presence of a large sinusoidal component at a frequency of 0.178 Hz, and that it was induced by feedwater controller action. The lesson to be learned here is that broad-band APD analysis is not always a valid indicator of core barrel motion.

Since the coherence, phase, and $|NCPSD_{12}(f)|$ data show that the pendulum-mode motion of the core barrel occurs in the 7- to 12-Hz frequency range, we constructed a second APD, using a signal band limited to approximately this frequency range (the actual range was 6.75 to 11.25 Hz) by a 24-dB/octave band-pass filter. This APD (Fig. 10) is more like a gaussian distribution, and, furthermore, its peak motion is

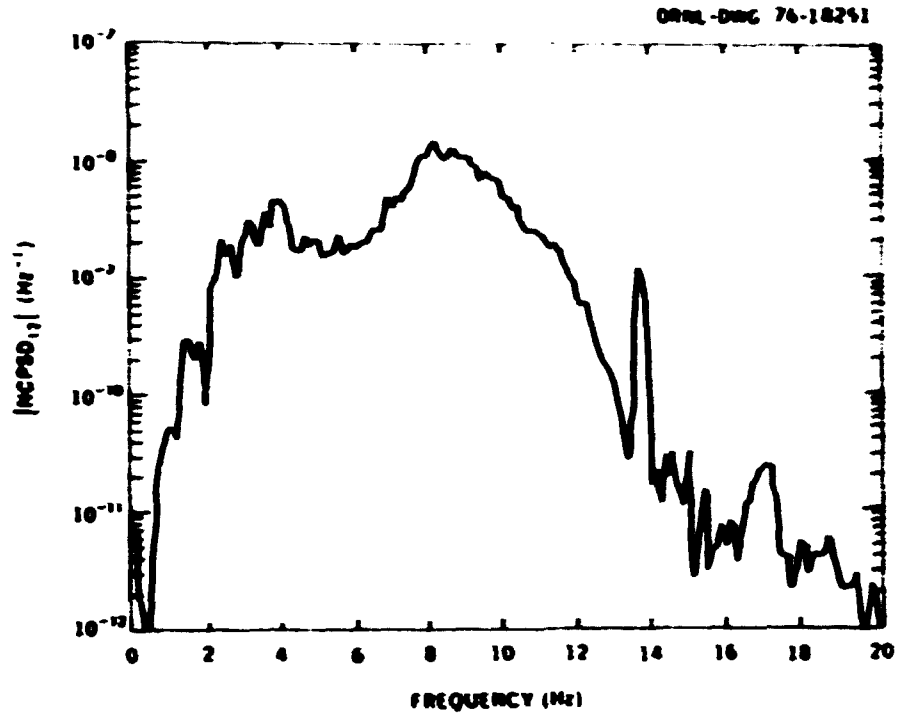

Fig. 8. |NCPSD| vs frequency (frequencies <2 Hz suppressed).

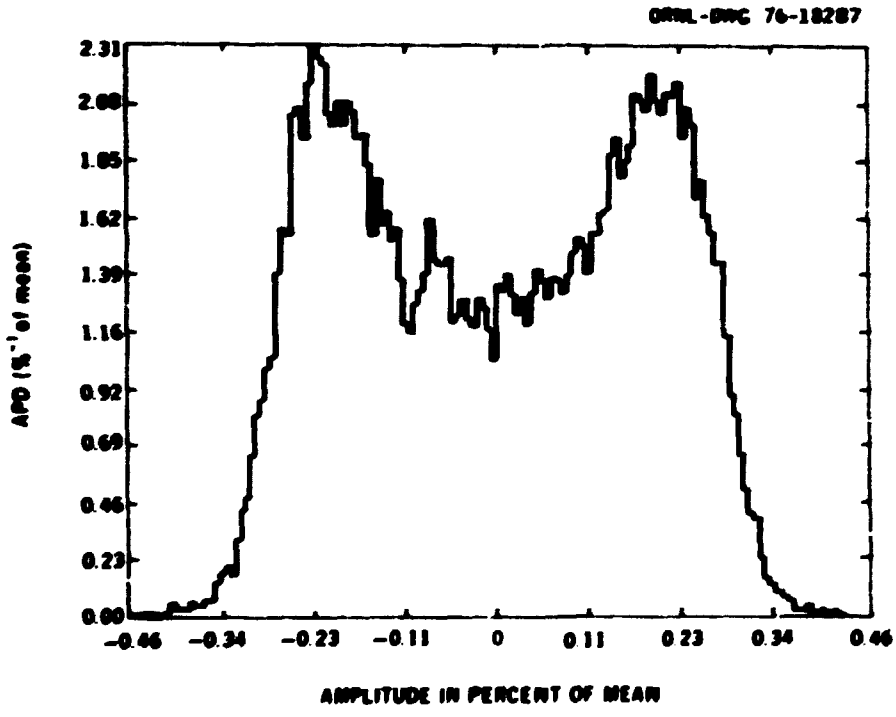

Fig. 9. Wide-band (6.75 - 11.25 Hz) amplitude probability density vs amplitude.

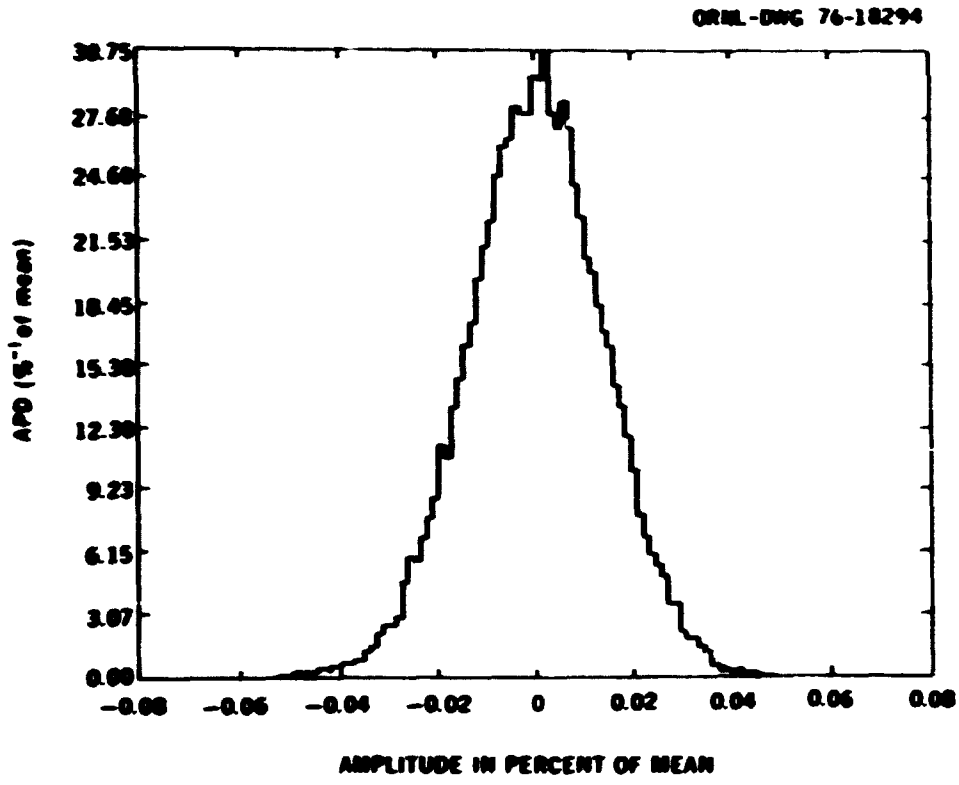

Fig. 10. Narrow-band (6.75–11.25 Hz) amplitude probability density vs amplitude.

~5–6 mils. which agrees with the earlier value obtained from the RMS value and a crest factor of 4.

The preceding comparison of the results from the two APDs emphasizes the importance of isolating the component of the fluctuating signal induced by core barrel motion before one constructs an APD for determination of core barrel motion. Fortunately, the core barrel motion component is usually found in a relatively narrow frequency band that can be separated from the frequency range of other components of the fluctuating signal. Therefore, this desired component can be obtained simply by passing the signal through an appropriate band-pass filter. Furthermore, as long as the coherence is large (greater than 0.7 or so), we can infer

core barrel motion from the signal from a single detector [the NPSD(f) or the band-limited APD]. We do not contend that the coherence will always be large; hence, in some cases the $|NCPSD_{12}(f)|$ data must be used to infer core barrel motion. The band-limited APD from a single detector will not be indicative of core barrel motion when coherence is small.

To conclude this discussion, the RMS motions inferred using Eq. (49) for several band-limited frequency bands are tabulated in Table 4. From these results, we conclude that there is not a great dependence on the statistical descriptor used (NPSD vs NCPSD); this is as would be expected, since the coherence is fairly high from ~4 to 13 Hz. Further, the results do not require great care in the selection of the bandwidth as long as the large contribution not attributable to core barrel motion at low frequencies (less than 2.0 Hz) is eliminated. If the bandwidth is ill-chosen, however (last entry of Table 4), inferred motion can easily be in error by an order of magnitude.

Table 4. Inferred core barrel motion

Frequency Band (Hz)	RMS Displacement[a] (mils)	
	NPSD	|NCPSD|
6.75 - 11.25	1.4	1.7
5.0 - 8.5	1.1	1.3
2.0 - 8.5	1.5	1.5
2.0 - 15.0	1.9	2.1
0.2 - 25.0	19.0	22.0

[a] An SF of 0.01% mil^{-1} was used.

6. CONCLUSIONS AND RECOMMENDATIONS

A two-dimensional model should be used to calculate the scale factor SF. A transport theory model of order P_1S_4 is sufficient. The calculation can be made as a shielding type (nonmultiplying medium) problem, using neutron cross-section sets readily available for shielding calculations; contributions from gamma rays can be ignored.

The results from four different analytical methods agreed reasonably well: forward direct, adjoint direct, adjoint difference, and adjoint difference approximate methods. From this variety, we demonstrated that the calculations had been performed to an acceptable degree of convergence and that a necessary assumption regarding the invariance of the SF with core barrel displacement (up to 500 mils) in the forward direct method was justified.

The SF calculated by the forward direct method for a detector at an angle θ (0 to 180°) relative to the assumed direction of motion of the core barrel showed that the SF varies approximately as cos θ for the detector at a fixed radial distance. The SF increases slightly with increasing radial distance into the biological shield (at least to 15 cm penetration) at a fixed angular location θ.

The application of the SF to the statistical descriptors NCPSD, NPSD, and APD demonstrated that core barrel motion cannot be inferred from broad-band APDs because these functions are sensitive to signal fluctuations from sources other than core barrel motion. The core barrel motion component of the fluctuating signal was identified from the coherence and phase functions in the frequency domain. The RMS value of the motion was

then obtained directly from the integral of the XCPSD function over the appropriate frequency range. Also, the peak value of the motion was obtained from the extrema of the APD function, constructed from a time signal that had been properly limited to this same frequency range that was characteristic of pendulum-mode motion, as identified from the coherence and phase functions. The RMS and peak values were shown to be consistent when a crest factor of 4 was assumed.

A significant result was the close agreement of the SF obtained from one-dimensional analysis (~0.04% per mil) with values commonly used in industry (~0.03% per mil), coupled with the result that our "best estimate" for the SF (from two-dimensional analysis: ~0.02% per mil at 0°) was ~2 times less than the value from one-dimensional analysis and ~1.5 times less than the value commonly used in industry. On this basis we concluded that it is not valid to compute the SF with a one-dimensional model and then assume a cos θ distribution to obtain results for two-dimensional applications, because the 0° value is so much in error.

A good deal of effort, including many cross-checks and determinations of internal consistency, went into this investigation to assure the accuracy of the resulting SFs. However, the use of a complex calculational model, plus the necessity of certain basic assumptions and a cross-section set, tend to cast some doubt on the results in spite of our precautions. Accordingly, we recommend that the two-dimensional calculated results be verified experimentally, following the extensive hot functional testing normally carried out on a "first-of-a-kind" plant.

7. ACKNOWLEDGMENTS

The authors thank D. N. Fry of ORNL for his many helpful suggestions and J. R. Penland (currently with the CRBRP project, Oak Ridge, TN 37830) and C. W. Mayo of The Babcock and Wilcox Company for their assistance in the early stages of this study.

8. APPENDIX: ENGINEERING DATA FOR TRANSPORT THEORY CALCULATION

The engineering data in this section were used to calculate the SF for a typical PWR.

One- and two-dimensional transport theory codes (ANISN and DOT) require detailed geometrical descriptions and component number densities. In the example calculation, a typical PWR with its associated external components is segmented into ten material zones as shown in Fig. 11. The number densities and the mesh sizing used in the calculation are given in Table 5, where most of the material number densities are from a typical PWR final safety analysis report. The mesh sizing in various zones was selected to ensure an optimum mesh spacing. The detector assumed was a $^{10}BF_3$ ionization chamber. The core radial power distribution which was used for the radial source distribution in the forward direct method of calculation (one- and two-dimensional calculations) is shown in Fig. 12.

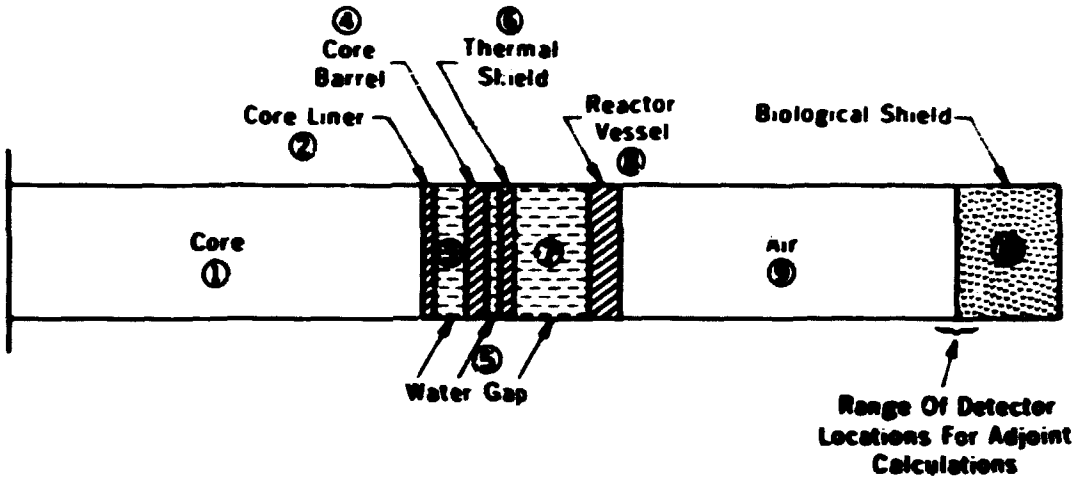

Fig. 11. Material configuration by zone number.

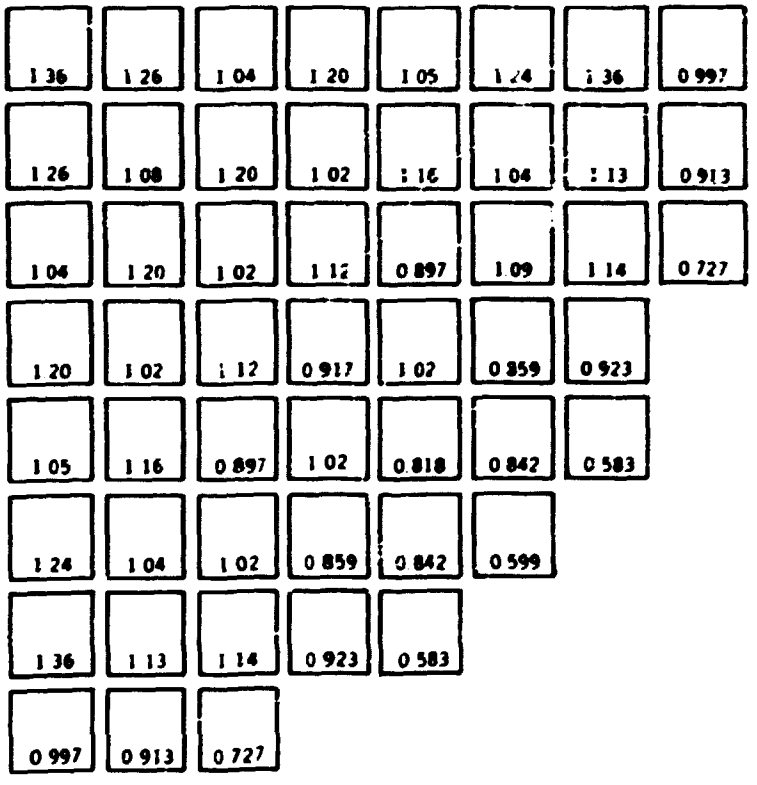

Fig. 12. Steady-state reactor radial power distribution for 100% full power (symmetric, 1/4 of the core is shown).

Table 5. Typical PWR engineering data

Zone and Component	Material	No. Density (atoms/barn-cm)	Mesh Spacing (cm)	No. of Mesh Points[a]
1			0 - 163.79	30 and 160[b]
Core	H	6.51769-2[c]		
	O[d]	3.25860-2		
	O[e]	4.55950-2		
	Zr	4.28770-2		
	^{235}U	6.72520-4		
	^{238}U	2.21250-2		
2			163.79 - 165.7	7
Core Liner	H	2.37670-4		
Steel	Si	8.89354-4		
	Cr	1.73856-2		
	Mn	1.51555-3		
	Fe	5.80720-2		
	Ni	8.50908-3		
3			165.7 - 179.07	15
Water and	H[d]	5.21367-2		
Steel	O	2.60688-2		
Spacers	H[f]	4.75340-5		
	Si	1.77871-4		
	Cr	3.47712-3		
	Mn	3.03110-4		
	Fe	1.16144-2		
	Ni	1.70182-3		
4			179.07 - 184.15	7
Thermal	Same as	Same as		
Shield	Zone 2	Zone 2		

Table 5. (continued)

Zone and Component	Material	No. Density (atoms/barn-cm)	Mesh Spacing (cm)	No. of Mesh Points
5			184.15 - 186.7	6
Water	H	6.51709-2		
Gap	O	3.25860-2		
6			186.7 - 191.77	7
Reactor	Same as	Same as		
Vessel	Zone 2	Zone 2		
7			191.77 - 217.17	30
Downcomer	H	6.51709-2		
	O	3.25860-2		
8			217.77 - 238.44	15
Core	C	8.67070-4		
Barrel	Al	7.01770-5		
	Si	4.26414-4		
	Cr	1.27455-4		
	Mn	1.12014-3		
	Fe	2.19792-2		
	Ni	4.83771-4		
	Ca	1.11749-4		
	Mo	2.71371-4		
9			238.44 - 350.53	10
Air	O	2.93780-5		
	N	7.34620-5		

Table 5. (continued)

Zone and Component	Material	No. Density (atoms/barn-cm)	Mesh Spacing (cm)	No. of Mesh Points
10			350.52 - 380	15
Biological	H	8.60386-2		
Shield	C	4.32885-2		
	O	1.15340-4		
	Na	1.23859-4		
	Mg	1.74103-3		
	Al	1.66180-2		
	Si	4.60522-4		
	K	1.50262-3		
	Ca	3.45087-4		
	Fe	9.64031-4		
Detector	^{10}B	4.2640-5		

[a] For one- and two-dimensional analyses except where noted.

[b] For one-dimensional analysis only.

[c] Read these numbers as 6.51769×10^{-2} .

[d] Coolant.

[e] Fuel.

[f] Steel.

9. REFERENCES

1. W. C. Pettus and R. L. Currie, "Monitoring Oconee I Internals with Neutron Noise Analysis," *Trans. Am. Nucl. Soc.* 19, 261 (1974).

2. Federal Register announcement of "Regulatory Guide of Core Barrel Motion Monitoring," *Fed. Reg.* 44(126), (June 30, 1975), p. 27508.

3. B. Oesterle, J. D. Kim, and H. Stölben, "Experimental and Theoretical Investigation of Flow-Induced Vibrations in Nuclear Components of PWR," Paper 527, International Symposium on Vibration in Industry, Keswick, England, April, 1973.

4. G. I. Bell and S. Glasstone, *Nuclear Reactor Theory*, Van Nostrand-Reingold, New York, 1970.

5. W. M. Stacey, Jr., *Variational Methods in Nuclear Reactor Physics*, Academic Press, New York, 1974.

6. W. W. Engle, Jr., *A User's Manual for ANISN: A One Dimensional Discrete Ordinates Transport Code with Anisotropic Scattering* K-1693 (1967).

7. F. R. Mynatt, *A User's Manual for DOT: A Two Dimensional Discrete Ordinates Transport Code with Anisotropic Scattering*, K-1694 (1967).

8. "CASK: 40 Group Coupled Neutron and Gamma-Ray Cross Section Data," Radiation Safety Information Center (RISC) Data Library Collection, DLC-23/CASK, Oak Ridge National Laboratory (1975).

9. G. E. Hansen and W. H. Roach, *Sixteen Group Cross Sections*, Los Alamos Scientific Laboratory Internal Report N-2-T53, Rev. 1 (1960).

10. D. E. Bartine, F. R. Mynatt, and E. M. Oblow, *SWANLAKE: A Computer Code Utilizing ANISN Radiation Transport Calculations for Cross Section Sensitivity Analysis*, ORNL-TM-3809 (1973).

11. R. L. Childs, *VIP, A Computer Program Using Two-Dimensional Discrete Ordinate Transport Calculation for Cross Section Sensitivity Analysis*, UCC-ND-CSD-1 (to be published).

12. D. R. Simpson, Neutron Physics Division, Oak Ridge National Laboratory, Personal Communication (1975).

13. J. S. Bendat and A. G. Piersol, *Random Data Analysis and Measurement Procedures*, Wiley Interscience, New York, 1971.

14. R. E. Uhrig, *Random Noise Techniques in Nuclear Reactor Systems*, Ronald Press, New York, 1970.

15. J. A. Thie, *Reactor Noise*, Rowman and Littlefield, New York, 1963.

16. J. C. Robinson, *Analysis of Neutron Fluctuation Spectra in the Oak Ridge Research Reactor and the High Flux Isotope Reactor*, ORNL-4149 (1967).